










Techno-Economic Analysis of Beam-Down Solar Tower Secondary Reflectors

Vishal Boga¹, Francisco Torres¹, Moritz Bitterling¹, Gregor Bern¹,
Peter Schöttl¹, Sophie Gledhill¹, Mario Magaldi², Mario Cilento²,
and Fulvio Bassetti²

¹ Fraunhofer Institute for Solar Energy Systems ISE, Germany

² Magaldi Power S.p.A., Italy

Abstract. Beam-down solar towers are presented as an alternative to conventional solar towers that allow modular design, easily adaptable to industrial environments. Secondary reflectors are a key component in this type of configuration, due to the high concentration of radiation received from the solar field. The results of a technical and economic study of new secondary reflectors, based on a polished stainless-steel substrate with silver PVD coating and a system of protective layers, are presented and compared with aluminum reflectors, currently used in such configurations. For this, twelve different designs, grouped in three cases are simulated using ray tracing and finite elements. The results show that the steel reflectors reach lower temperatures compared to aluminum reflectors, allowing for greater durability. Additionally, the optical efficiency of the plant was determined, and it was estimated that steel reflectors can reduce the LCOH of the plant by approximately 3.5%.

Keywords: Beam-Down, Secondary Reflector, Solar Tower, FEA, Ray Tracing, LCOH

1. Introduction

Concentrating beam-down solar towers (BDST) have several advantages over state-of-the-art solar towers, especially the ground-based receiver. Its possible integration with the thermal storage is regarded as a promising simplification for the integration in industrial processes or modular power plants. Heliostats concentrate the sun to the receiver via a secondary reflector, installed at elevated position. The reflectance, shape and durability of the secondary reflector play a major role for the efficiency of the beam-down power plant, while increased concentration and lightweight design are challenging conditions for the component. In existing systems, aluminum reflectors are used, which have a solar-weighted specular reflectance of about 90%. The aluminum limits the reflectance as well as the operating temperatures to below 473 K. In the SOLBEADO project [1], polished steel with silver physical-vapor-deposition (PVD) coated reflectors are in development to improve both aspects: on one hand, an increase in reflectance to at least 93%, and on the other hand, durability at higher operating temperatures.

The purpose of this publication is to demonstrate the positive technical and economic impact of the implementation of steel reflectors by using Finite Element Analysis (FEA) and ray tracing simulations. For this, calculations of the solar flux density on the secondary reflectors, of the resulting temperature profile on its surface, of the deformation caused by

temperature changes and by gravity, of its impact on the optical efficiency and of the Levelized Cost of Heat (LCOH) for six different reflector designs are carried out.

2. Methodology

To calculate the LCOH of the BDST (Fig. 1), the first step is to calculate the maximum incident solar flux on the surface of the secondary reflectors via a ray tracing simulation using the in-house Fraunhofer ISE tool Raytrace3D [2]. Concentration maps on the secondary reflectors are derived for several sun positions at a given location. The maximum concentration is used as input to FEA, allowing to determine the deformation of twelve secondary reflector designs due to temperature and gravity. Subsequently, the local slope deviations of the reflector surfaces are calculated and imported back into Raytrace3D to compute the impact of the gravitational and thermal deformation on the optical efficiency of the BDST plant. Finally, a techno-economic analysis is carried out considering the manufacturing cost of the secondary reflectors and the calculation of the optical efficiency of the plant, allowing to obtain the LCOH of the different designs used.

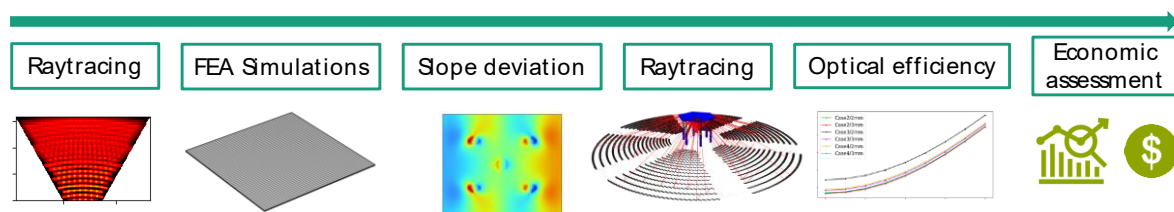


Figure 1. Methodology for the techno-economical assessment using ray tracing and FEA simulations.

2.1. Ray tracing

The Fraunhofer ISE in-house simulation tool Raytrace3D [2] is a ray tracing engine based on the Monte-Carlo method, which allows the analysis of energy transmission within concentrating collector systems. Raytrace3D is a flexible program containing different modules for geometrical modeling, which considers several optical loss mechanisms as tracking errors, atmospheric attenuation, shading, spillage and reflector surface errors.

The model scene in Raytrace3D consists of a solar field of approximately 12000 m², a tower of 33 m meters high, which holds a secondary reflector area of 1580 m², and optically relevant structural elements. The reflectance of the heliostats is 92.2%, while the reflectance of the stainless-steel secondary reflectors is 93% and that of the aluminum reflectors is 90%. The circular receiver has an aperture width of 2.2 m. The sun is described with the Buie/Neumann model. In Fig. 2, the ray tracing scene is depicted. The simulation is run for 100 representative solar zenith/azimuth combinations to find the largest concentration value on the secondary reflectors that occurs during operation.

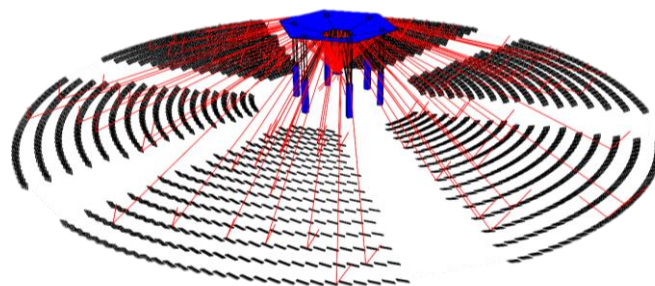


Figure 2. Beam Down Solar Tower scene in Raytrace3D.

For the first step, the ray tracing simulations are adapted to represent the extreme case regarding concentration on the secondary (clean heliostats with zero mirror errors, low

circumsolar radiation, no atmospheric attenuation). A concentration map of the surface of the secondary reflector array is obtained for the different solar angles. The maximum value is used as an input of the FEA Simulations. From these, the deformation and the local slope deviations are computed.

Once the finite element simulations have been carried out, a second ray tracing simulation is performed, this time with realistic (instead of extreme case) parameters including the local slope deviations in the secondary reflectors. The scene of the ray tracing simulations is identical to the one mentioned above, only that in this second simulation, when the rays interact with the secondary reflector surface, the ideal surface normal is replaced by the local normal defined by the slopes coming from the FEA simulations. This allows to account for the optical losses of the secondary reflectors due to gravity and thermal deformation. The loss or increase in optical efficiency will be considered for each design model in the economical assessment.

2.2. FEA Analysis

Secondary reflectors can be attached to the tower using different fixation supports. The optimal support structure to suspend the secondary reflectors on the tower minimizes the reflectors slope deviation, which is occurring due to gravity, wind loads and deformation due to temperature gradients. Twelve designs for the secondary reflectors are analyzed using FEA.

The new studied stainless-steel secondary reflectors coated with a PVD silver layer of thickness >100 nm embedded in barrier and adhesion layers deposited using PVD, plasma-enhanced chemical vapor deposition (PE-CVD) and/or plasma-enhanced atomic layer deposition PE-ALD. Silver-coated secondary reflectors have a solar-weighted reflectance of 92 to 96%. For this study, a reflectance of 93% is assumed. The state-of-the-art reflectors are made of aluminum including a reflective layer, which have a reflectance of 90%. For simulations, the dimensions of the square secondary reflector panels are 0.85×0.85 m² and thickness of 2 mm and 3 mm.

In total, three design cases are studied, each of them with 2 mm and 3 mm reflector thickness:

- **Case 1: Five welded brackets:** In case 1, the supports used are 2mm thick steel bend plates with a height of 150 mm and a width of 60 mm. The supports are welded on the top surface of the reflector (Fig.3A).
- **Case 2: Four supports:** In case 2, the reflector is cut at the center of each edge with a length of 15mm and is bent above to attach the steel bend plate support. The steel bend plate support dimensions used in this case have a height of 0.15 m, a width of 15 mm, and a thickness of 1 mm (Fig. 3B).
- **Case 3: Four support at edges and one central bracket:** Case 3 is similar to case 2, but one support is welded at the center of the reflector (Fig. 3C).

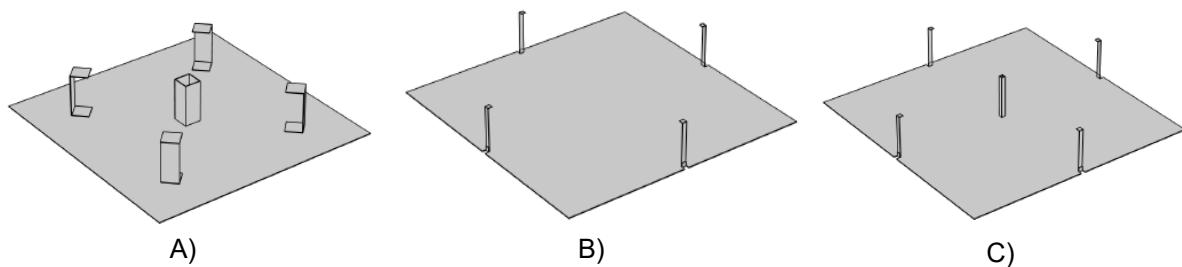


Figure 3. Possible designs of the suspension structure of the secondary mirror. A) Case 1, B) Case 2, C) Case 3.

The material properties are presented in Table 1.

Table 1. Physical properties of stainless steel and aluminum.

Properties	Stainless-steel	Aluminum	Unit
Density	8000	2700	Kg/m ³
Specific heat capacity	460	900	J/Kg K
Thermal conductivity	16.2	238	W/m K
Thermal Expansion Coefficient	17.2 x 10 ⁻⁶	23 x 10 ⁻⁶	1/K
Young's Modulus	192 x 10 ⁹	70 x 10 ⁹	[Pa]
Poisson's ratio	0.265	0.33	-
Emissivity	0.44	0.11	-

The boundary conditions of the study are:

- Gravity: Including all the elements of the reflector.
- No displacement: At the end of the welded brackets and supports.
- Incoming solar radiation: Maximum concentration obtained from the ray tracing simulations and applied over the surface of the reflector. The concentration is multiplied by the DNI (1000 W/m²) and by the absorptance of the reflector (7% for the silver coated stainless-steel and 10% for aluminum).
- Convective heat losses: Only natural convection was assumed for all surfaces of the reflector, including the supports and brackets. This is the "worst-case" scenario, as the maximum reflector temperature occurs when there is no wind.
- Radiative heat losses: Applied in all the surfaces. The thermal emissivity is set to 12% for the aluminum reflector and 2% for the silver coated stainless-steel reflector. This is due to the reflective coating of the surfaces.

The results of the FEA simulations are used as an input for the next ray tracing simulations. Specifically, the local slope deviations are exported from the surface of the reflector, so that the surface normal can be locally modified, and therefore, the deformations of the reflector are considered in the ray tracing, impacting directly the optical efficiency of the system.

2.3. Economic assessment

For the economic analysis, estimated values for the investment cost of the solar field, tower structure, secondary reflectors, receiver, as well as operation and maintenance costs are used.

The LCOH is calculated with equation (1):

$$LCOH = \frac{CAPEX + OPEX \cdot LVF - \frac{Salvage}{(1+r)^i}}{Production \cdot \frac{(1+r)^i - 1}{r(1+t)^i}} \quad (1)$$

Where the CAPEX is the investment cost of the solar field, storage unit, solar tower including the secondaries and receiver, the OPEX are the operational expenditures, the salvage is the value of the assets at the end of the project lifetime and the production is the annual heat produced. The discount rate and project lifetime are r and i respectively.

For each case studied, the heliostat field, receiver, solar tower, and thermal storage costs remain equal. The only parameters that vary are the costs of the secondaries and the optical efficiency of the plant for every different secondary case.

3. Results and discussion

3.1 Concentration

Fig. 4 shows the concentration map of the secondary reflectors for the cases of zenith angle 21.6° and azimuth angle 110.8° . Each trapezoid represents one of the six segments of the secondary reflectors divided into the azimuthal sectors 0° , 60° , 120° , 180° , 240° and 300° .

For this specific solar position, the maximum concentration on the surface of the secondary reflectors is obtained, reaching 19.5 suns in the 120° segment. The maximum average concentration, however, is found in the 300° segment, reaching 6.6 suns.

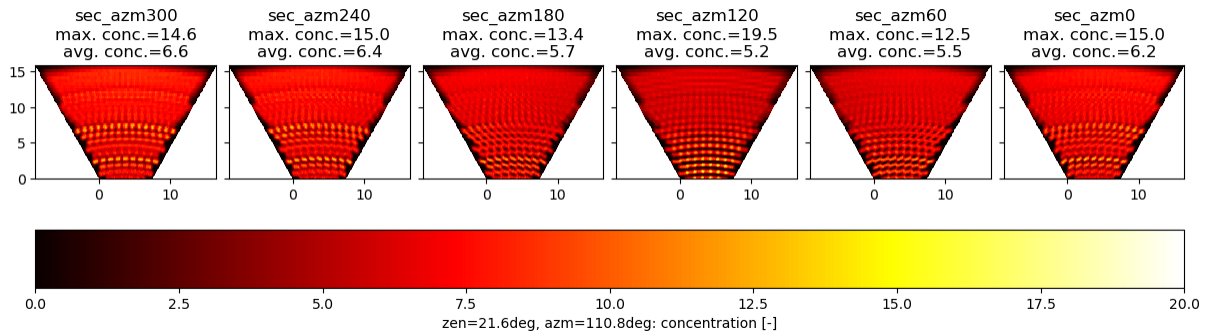


Figure 4. Concentration map of secondary reflectors at zenith angle 21.6° and azimuth angle 110.8° sun position. From left to right the 6 segments of the secondary reflectors: 300° , 240° , 180° , 120° , 60° and 0° azimuth.

3.2 Temperature on the surface

The maximum concentration used to determine the maximum temperature the reflector can reach is 25 suns, more than the maximum value found of 19.5. This is considered an additional safety factor, as the concentration may increase due to improperly calibrated heliostats or overlaps for short periods of time due to heliostat movement.

The temperature profile of 6 design cases (2 mm thickness) are presented in Fig. 5. The largest temperature of 466 K is reached by the aluminum reflector case 2, being close to the maximum stability temperature of the reflector (473 K). The steel reflectors present lower maximum temperature (405 K for case 2) on the surface of the reflector, mainly due to the higher reflectance and emissivity. This allows potentially to increase the concentration on the secondary reflectors, and therefore a larger solar field is possible to be installed. In addition, they also show a larger temperature difference ranging from 28 K to 31 K, while the aluminum reflectors range from 12 K to 14 K, due to the better heat conduction.

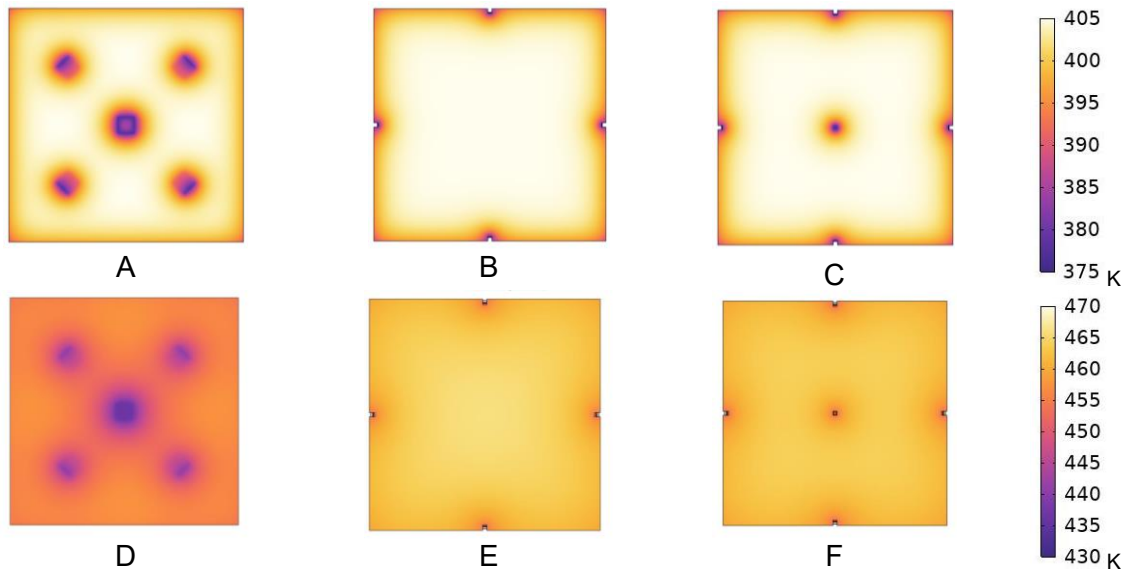


Figure 5. Temperature profile in Kelvin of one secondary reflector facet simulated at 25 suns. A) Case 1, 2 mm thickness stainless steel; B) Case 2, 2 mm thickness stainless steel; C) Case 3, 2 mm thickness stainless steel; D) Case 1, 2 mm thickness aluminum; E) Case 2, 2 mm thickness aluminum; F) Case 3, 2 mm thickness aluminum.

3.3. Slope deviation X direction

Temperature and gravity cause deformation on the surface of the secondary reflectors. Their effect can be seen in Fig. 6, which shows the local slope deviation in x direction (sd_x) in mrad (the case in Y direction is analogous). The design of case 1 has the lowest sd_x due to its 5 points of fixation of the structure. Case 2 has the highest sd_x because there is no fixation at the center of the reflector, and therefore gravity increases the deformation at the surface. Case 3 has deformations at an intermediate point between case 1 and 2.

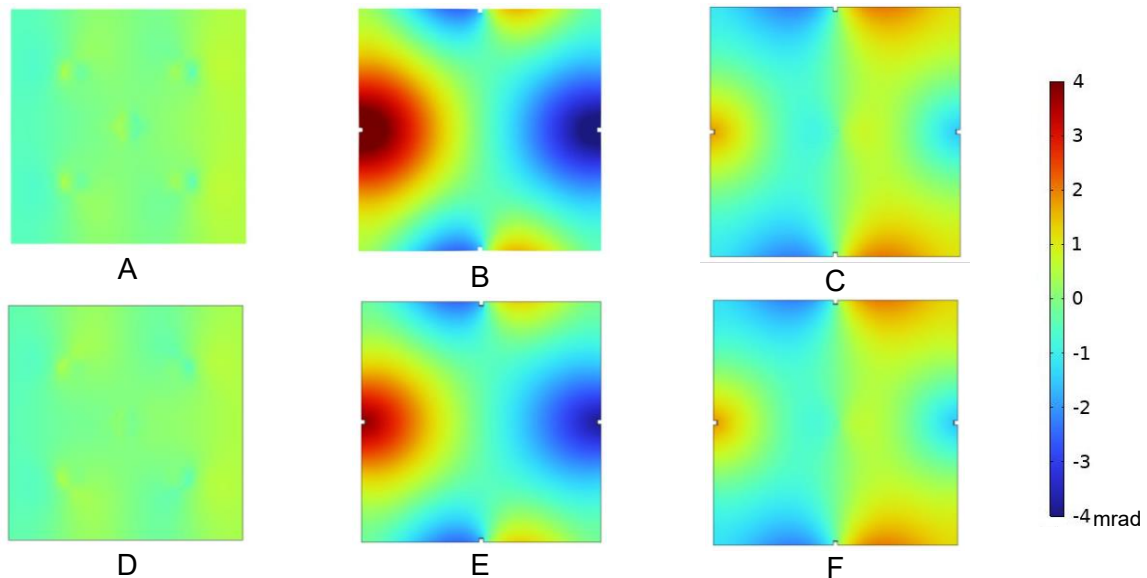


Figure 6. Local slope deviation in mrad of a secondary reflector facet simulated at 10 suns and gravity load. A) Case 1; 3mm thickness stainless steel. B) Case 2; 3mm thickness stainless steel. C) Case 3; 3mm thickness stainless steel. D) Case 1; 3mm thickness aluminum. E) Case 2; 3mm thickness aluminum. F) Case 3; 3mm thickness aluminum.

In Table 3, the Root Mean Square values of the local deviations of the slope in x direction (SD_x) are presented. Case 1 presents low values of up to 0.56 mrad, while the case 2 reflector (2 mm thick stainless steel) slightly exceeds 4 mrad. Case 3 has intermediate values between 0.9 and 2 mrad approximately.

Table 2. RMS of local slope deviation in x direction in mrad for every design reflector case.

Case	Steel RMS X (mrad)	Aluminum RMS X (mrad)
Case1 2mm	0.54	0.56
Case1 3mm	0.27	0.22
Case2 2mm	4.03	3.61
Case2 3mm	1.86	1.62
Case3 2mm	2.04	1.99
Case3 3mm	0.9	0.89

3.4 Optical efficiency

After calculating the local slope deviations, the ray tracing is used to estimate the optical efficiency of the secondary reflectors. The results are shown in Fig. 7. The reflectors with a thickness of 3 mm have a higher or equal optical efficiency than the 2 mm reflectors due to their lower deformation, and consequently lower SDx. In case 1 of stainless steel for 2 and 3 mm the efficiencies are almost equal due to their low SDx. BDST using aluminum reflectors have in all cases lower optical efficiency than stainless steel reflectors, mainly due to the 3% increase in reflectance of the stainless-steel reflectors. For both, the stainless-steel and aluminum, case 1 has the highest efficiency, while case 2 has the lowest efficiency.

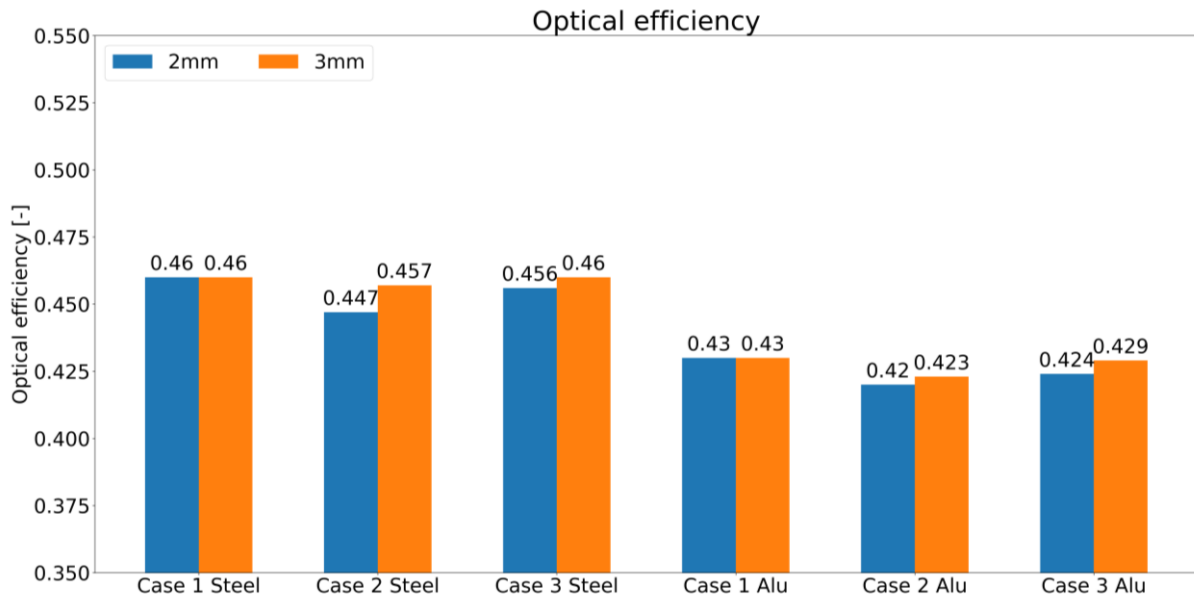


Figure 7. Optical efficiency for the stainless-steel and aluminum reflectors.

3.5 Economical assessment

Fig. 8 presents a relative comparison between the LCOH of the aluminum and steel secondary reflector cases. A negative value means that the steel has a lower LCOH than the aluminum reflectors case, while a positive value means that the aluminum case has lower LCOH than the steel case. From this figure, all the investigated cases have a lower LCOH for the steel reflectors, reaching a maximum decrease of -3.5 % in case 1 for 2 mm reflector thickness and a lowest decrease of -2.9 % in case 2 for 2 mm reflector thickness. The average reduction of LCOH when using stainless-steel reflectors compared to aluminum reflectors is 3.2 % for 2 mm thickness reflectors and 3.1 % for 3 mm thickness reflectors.

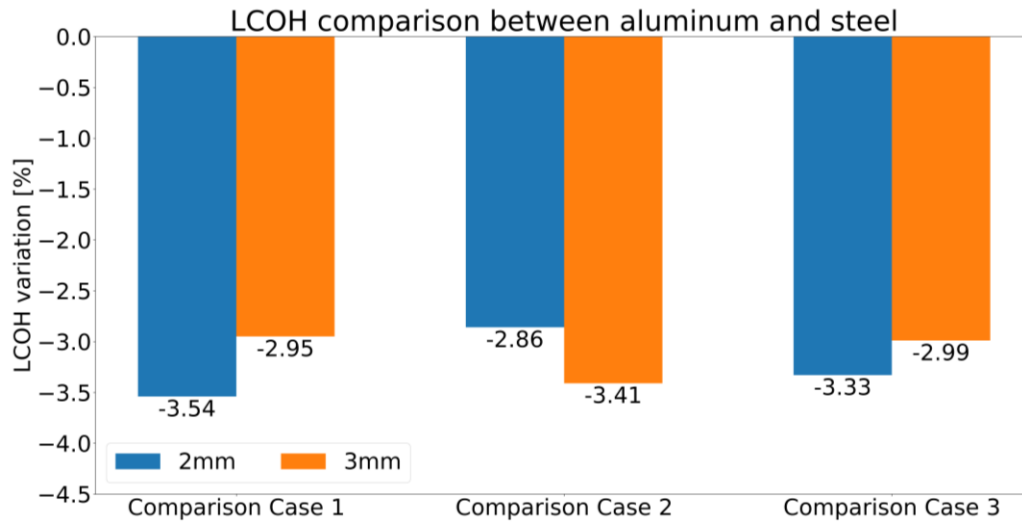


Figure 8. Levelized Cost of Heat comparison between aluminum and stainless-steel reflectors. A negative value represents a lower LCOH for the stainless-steel reflectors.

4. Conclusions

A technical study of 12 types of secondary reflectors of a beam-down solar tower was carried out. For this, the solar concentration on the surface of the reflectors was determined, obtaining a maximum of 19.5 suns. Additionally, it was established that the maximum temperature that the stainless-steel reflectors can reach is 405 K, which is 61 K lower than the aluminum reflectors. This implies that the solar field can be enlarged if the steel reflectors are used. The impact of temperature gradients and gravity on the deformation of the reflectors was also determined. Case 1 presented maximum SDx values of 0.56 mrad, case 2: 4.03 mrad and case 3: 2.04 mrad. With the local slope deviation maps, the optical efficiency of the plant was calculated, reaching a maximum of 46%. Finally, an economic analysis was performed, establishing that stainless-steel reflectors can reduce the LCOH up to 3.5% compared to aluminum reflectors.

Data availability statement

The information on which this publication is based is confidential and therefore not publicly accessible.

Underlying and related material

The authors of this publication found no similar publications on the topic to be presented in this section.

Author contributions

Vishal Boga, Francisco Torres, Moritz Bitterling, and Peter Schöttl: Conceptualization, Formal Analysis and Investigation.

Sophie Gledhill and Gregor Bern: Funding acquisition, Project administration and Supervision.

Mario Magaldi, Mario Cilento, and Fulvio Bassetti: Resources and Validation.

Competing interests

The authors declare that they have no competing interests.

Funding

The project SOLBEADO, under which the work presented in this paper has been conducted, is funded by the German Federal Ministry for Economic Affairs and Climate Action (BMWK) under grant 03EE5083A. The authors of this publication are responsible for its contents.

References

1. Fraunhofer Institute for Solar Energy Systems ISE, "SOLBEADO – Development and testing of secondary reflectors for a beam-down tower power plant," April 2023. [Online]. Available: <https://www.ise.fraunhofer.de/en/research-projects/solbeado.html>.
2. Schöttl, P.; Bern, G.; Nitz, P.; Torres, F.; Graf, L. (2022): Raytrace3D by Fraunhofer ISE. Accurate and Efficient Ray Tracing for Concentrator Optics. Online <https://www.ise.fraunhofer.de/content/dam/ise/de/downloads/pdf/raytrace3d.pdf>.